ISSN: 0369-8963

Effect of heat treatment temperature on whitlockite prepared using Dolomite

NANTHINI AMIRTHALINGAM[1)], THENMUHIL DEIVARAJAN[1)]*, MANOHAR PARAMASIVAM[1)]

1) Department of Ceramic Technology, Alagappa College of Technology, Anna University, Chennai 600 025.

**Corresponding Authors Email: *thenmuhil@annauniv.edu*

Tel: 044 2235 9200.

Abstract

Whitlockite (WH) is a significant calcium phosphate (CaP) material due to its surprising biological properties. Much work has been done on different CaPs like hydroxyapatite and β-tricalcium phosphate which are not hard to synthesize. In this study, we are revealing an easy union strategy for WH synthesis, utilizing dolomite, by precipitation. The objective was completed by stirring, aging, and heat treating the obtained powder at different temperatures, with practically no medium, under the ambient environment. The powder gotten was analyzed by thermogravimetric (TGA), x-ray diffraction (XRD), Fourier changes infrared spectroscopy (FTIR), Scanning electron microscopy (SEM), anti-bacterial test, and protein adsorption. XRD examination affirmed that the obtained material is whitlockite. The in-vitro tests proved that the obtained WH is biocompatible. The technique gives simple method for large-scale manufacturing of WH.

Key words: Dolomite; Precipitation; sintering; whitlockite; XRD

Introduction

Natural hard tissues keep their health throughout their lifetime by self-regenerating their micro-damaged parts through a bone remodelling process. Whitlockite (WH-$Ca_{18}Mg_2H_2(PO_4)_{14}$), the second most abundant biomineral in human bones, has gotten a lot of attention recently because of its superior bone tissue regeneration ability when compared to other calcium phosphates (CaPs) like hydroxyapatite (HA) and beta-tricalcium phosphate (β -TCP) [1]. It is more capable of differentiation and proliferation. WH is distinguished from HA by the presence of Mg^{2+} ions in its distinct crystal structures. More than half of the Mg^{2+} in the human body is stored in bone tissue, which is required for proper skeletal, nervous, and muscular system function. Mg^{2+} ions, free from WH, in the surrounding area of implants placed in osteoporotic bone, for example, have been shown to stimulate human turbinate-derived mesenchymal stem cells to persuade osteogenic differentiation while preventing osteoclast differentiation from monocytes. Furthermore, Mg^{2+} release promotes rapid bone formation and anabolic marker expression in the peri-implant bone [2-5]. Human dentin consists of approximately 26 to 58 wt% WH and it contributes a maximum of 20% of bone tissues. The proportion of WH in hard tissue has been reported to be higher in the younger ages and earlier stage of mineralization. In spite of its usefulness, problems persist in WH synthesis and difficulties in its detection. Many earlier studies have concentrated on the role of Mg^{2+} in HA synthesis. Direct synthesis of WH is very difficult at higher temperature or it is difficult to dope Mg^{2+} into HA. Doping Mg^{2+} into HA is difficult due to the atomic radius difference between Mg^{2+} and Ca^{2+}, and doping has been shown to significantly manipulate the morphology, crystallinity, and growth rate of HA. Mg^{2+} has been reported to inhibit the formation

 https://doi.org/10.37896/pd91.3/9134

ISSN: 0369-8963

of crystallization of dicalcium phosphate dihydrate (DCPD), and octacalcium phosphate (OCP) by getting adsorbed at their crystal surface and disturbing their atomic arrangement. In calcium-phosphate materials, the substitution of Mg^{2+} for Ca^{2+} decreases the size of the unit cell of apatite lattice giving rise to an apatite with low crystallinity.

Despite their enormous potential, WH crystals have been moderately neglected in bone regeneration research due to difficulties in artificial synthesis inspite of its presence in living organisms. However, a few other reports have been published in recent years as a result of Rowles' pioneering work on the preparation of WH [5]. Calcium phosphate can be prepared by several synthetic routes which include precipitation, sol-gel processes, hydrothermal method, spray pyrolysis from natural coralline, and solid state reaction. Among these techniques, the most widespread is the precipitation process. However, the composition, crystal size, physicochemical properties and morphology of synthetic apatites are sensitive to preparative conditions and at times it resulted into non-stoichiometric calcium deficient powders. The cost of the process can be minimized by using low cost raw material [6]. Dolomite is a natural raw material and has hexagonal crystal structure. It is used as a major refractory oxide in the refractory industry. Dolomite is $CaMg(CO_3)_2$ and its thermal decomposition occurs in two stages: (i)700°C and (ii)900°C [7]. During the calcinations process the carbonates in dolomite is decomposed into CaO and MgO thus eliminating CO_2 [8] and calcined dolomite is called doloma. Presence of MgO also acts as a sintering additive, and Mg was reported to stabilize β phase of TCP [9]. In this work, dolomite was converted to doloma and used as calcium source with diammonium hydrogen phosphate as phosphorous source for preparation of whitlockite ceramic material by precipitation method with high temperature stability.

Experimental procedure

Dolomite was placed in muffle furnace at 1000°C, with a heating rate of 5°C and 2 h soaking to convert it to doloma (CaO.MgO). Doloma suspension and diammonium hydrogen phosphate solution were prepared separately using distilled water. Appropriate amount of diammonium hydrogen phosphate was mixed with the calcium precursor by stirring homogenously. The mixed precursors were aged for 48 h at room temperature. The white precipitate obtained was filtered and washed for 2 to 3 times using distilled water. The washed precipitate was placed in dryer for 24 h at 110°C. Pellets with ~2 mm thickness were made using dried powder in an uniaxial press employing a load of about 150 MPa. The dried powder and pellets were finally subjected to sintering in a muffle furnace at temperatures from 900°C to 1200°C, with heating rate of 3°C/min and soaking for 2 h at maximum temperature.

Characterization techniques

The phase compositions of the prepared and sintered samples were characterized using X-ray powder diffraction (XRD) (BRUKER USA D8 Advance) in 2θ range from 10 to 90 Degrees. The crystallite size was calculated by using Scherrer Equation $D_s = \frac{k\lambda}{\beta\cos\theta}$, where k is a costant equal to 0.9 , λ is the X-ray wavelength, θ is the Bragg's diffraction angle (in degrees) and β is the full-width at half maximum of X-ray reflection (in radian). Fourier-transform infrared spectroscopy (FTIR) (Perkin Elmer) was done in the range of 4000-400 cm^{-1}. Thermal studies were performed on prepared powders using a heating rate of 10°C/min up to 1200 °C in Perkin Elmer TG/DTA analyzer. Density was measured by the Archimedes method and Hardness (Zwick) done by

 https://doi.org/10.37896/pd91.3/9134

ISSN: 0369-8963

Vicker's Hardness (Hv) method. The morphology of sintered powder and pellet was observed using a scanning electron microscope (SEM) (Thermosceintific Apreo S). For *in-vitro* studies, pellets sintered at 1200°C were placed in HBSS solution at 37°C for 7 and 14 days to analyze the bioactivity. After the respective immersion times, the samples were washed in deionized water and dried at room temperature. Antibacterial activity of 900°C to 1200°C sintered samples was tested against gram-negative pathogenic bacteria namely *Escherichia coli* (E.Coli) and the standard disc diffusion method was used to assess antibacterial activity. WH sintered samples were added onto the plate. The plates were incubated overnight at 37°C and observed for inhibition of the bacterial growth around the pellets. For protein adsorption experiments, Bovine serum albumin (BSA) was chosen as the protein, and concentrations were assayed using the Bradford protein assay method. The 1200°C sintered powder was immersed in 1mL of aqueous solution with a constant concentration of BSA (1mg mL-1) for different times (1hour, 2hours, and 4hours). The solution was agitated in a vibrator at a constant temperature (4°C). For the triplicate test, 100µl of sodium dodecyl sulfate (SDS) solution (1%) was added to the plate containing the samples.

Results and discussion

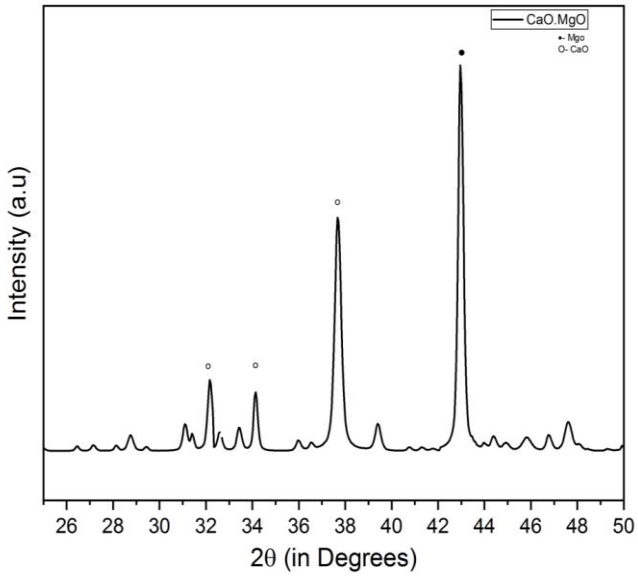

Figure 1. XRD image of Calcined dolomite

The formation of doloma CaO.MgO peaks were detected at 32.3° and 37.4° which corresponds to the calcium oxide (JCPDS file no. 82-1691) generated by (111) and(200) reflections, respectively. Meanwhile, the peak at 42.9° corresponded by (200) reflections (Fig.1) was the characteristic peak of magnesium oxide (JCPDS file no. 78-0430). The total mass loss of the precipitated sample was 21.99% (Fig.2). Three stages of weight loss, as observed from the TGA curve, are at T<200°C and at 200°C<T>800°C. Initial weight loss was due to removal of absorbed water molecules from the samples. Larger amount of weight loss was due to removal of organic content and residue like ammonia from the prepared samples at T>200°C.

 https://doi.org/10.37896/pd91.3/9134

ISSN: 0369-8963

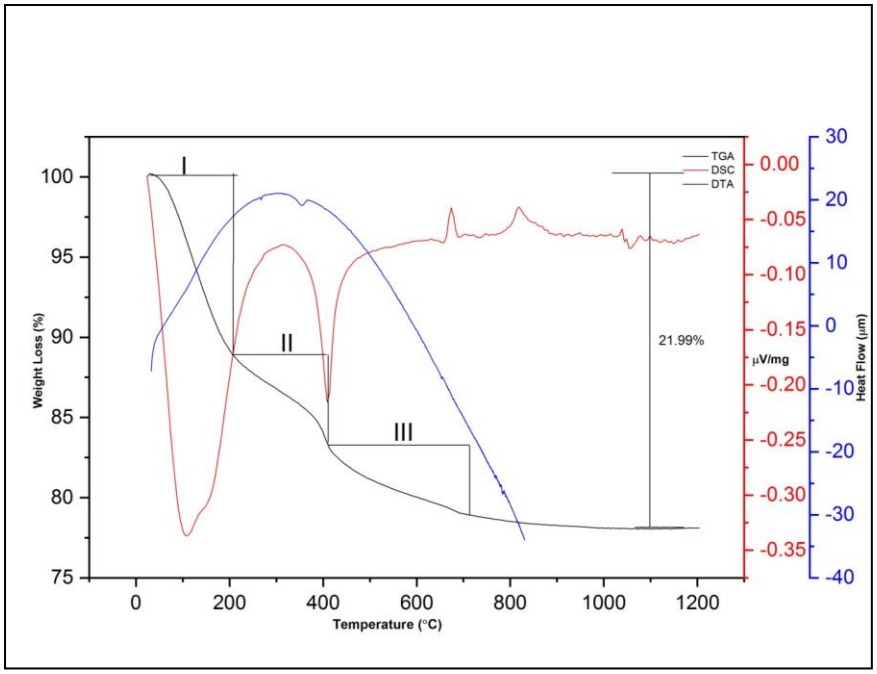

Figure 2. TGA-DTA-DSC curve for precipitated powder

Figure 3 shows XRD patterns of the sintered WH powder. The most intensive diffraction peaks for WH, HA and TCP were recorded in 2θ range 25-45° (Fig.3). The lower temperature peaks indicated the formation of WH phase. A significant increase in WH peaks intensity was recorded with increase in temperature and correspondingly HA phase intensity decreased. This increase in intensity of WH peaks confirmed that the formation and crystallization of WH was enhanced as temperature increased. Sintered samples at 1200°C showed well crystallized WH phase and peaks (1010), (124), (0210),(220),(2110) and (2112) matched with the standard JCPDS 70-2064 [10]. The most intense diffraction peaks corresponding to CaO and MgO (Fig.1) disappeared on heat treatment. XRD patterns of sintered samples showed the presence of WH with rhombohedral structure, HA and β-TCP phases only. Generally, the preparation process, impurities from phosphorus and pH control are critical parameters in precipitated synthesis, and the XRD analysis gave results with no observable other CaPs (TTCP, DCP, etc.,) in the investigated samples.

Table 1. Crystallite size, Lattice parameters and cell volume of sintered samples

Temperature (°C)	Crystallite size (nm)	Lattice Parameters		Cell Volume
		a (Å)	c (Å)	V(Å^3)
900	17.46	10.354	37.04	3439.22
1000	19.49	10.355	37.05	3440.37
1100	21.3	10.355	37.07	3442.17
1200	35.17	10.361	36.99	3438.52

The crystallite size, lattice parameters and unit cell volume of samples was calculated for different sintering temperatures and are mentioned in Table 1. The incorporation of Mg^{2+} into CaP was reflected in the shift of the XRD peaks caused by partial Mg-for-Ca substitution, which

 https://doi.org/10.37896/pd91.3/9134

ISSN: 0369-8963

resulted in a contraction in the cell volume and structure stabilisation. All sintered powders were crystalline with apatite structure. It can be seen that the diffraction peaks became narrower and sharper with increasing sintering temperature. This indicates that the crystallite size of the WH increases when sintering temperature is increased from 900°C to 1200°C.

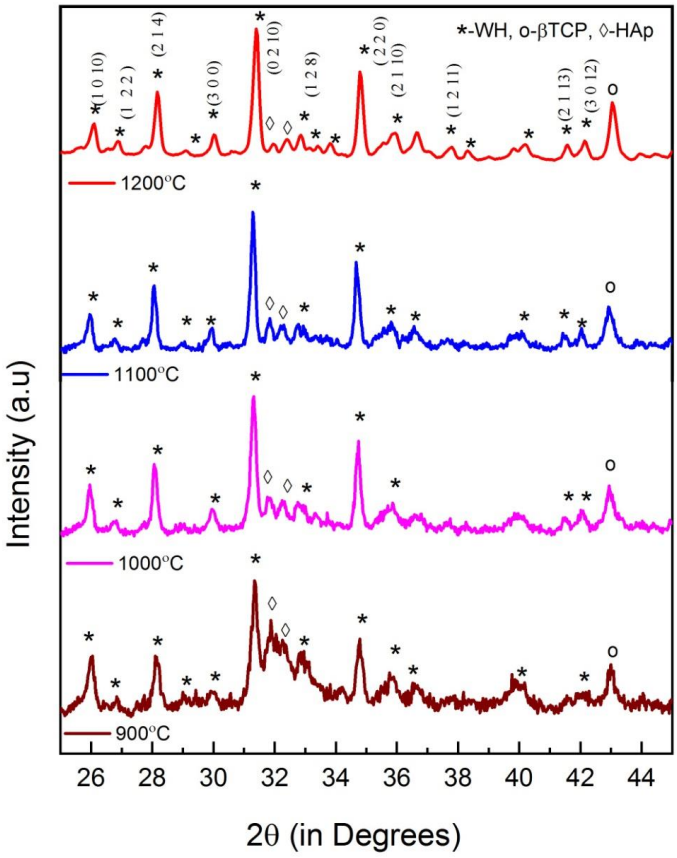

Figure 3. XRD pattern of the sintered powders

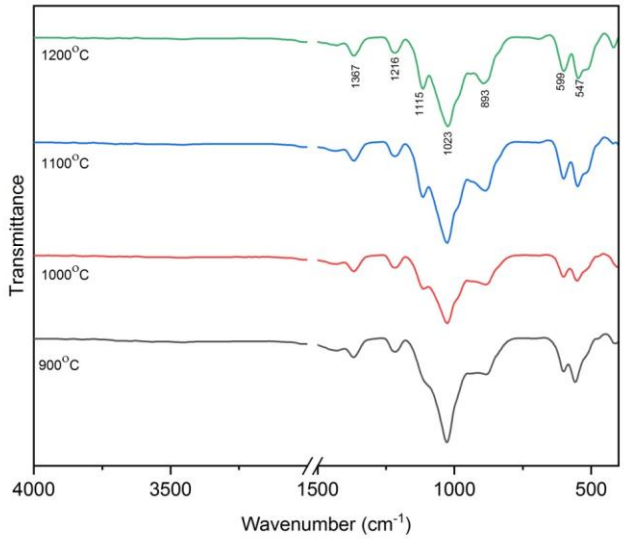

Figure 4. FTIR pattern of the precipitated powders sintered

https://doi.org/10.37896/pd91.3/9134

ISSN: 0369-8963

The FTIR spectra of sintered samples at different temperatures and vibrational modes characteristic of PO_4^{3-} are shown in Figure 4 It was found that all sintered samples, show phosphate in IR spectra. The bands at 547cm^{-1}, and 599cm^{-1} were assigned to the O–P–O bending mode (ν_4) [11]. The HPO_4^{2-} vibrational stretching was observed in the band 893 cm^{-1}. The bands of 1023 cm^{-1} and 1115 cm^{-1} are related to the PO_4^{3-} vibrational stretching. FTIR analysis of bone done by Boskey and Camacho showed the presence of major inorganic species, phosphate and carbonate gatherings (from HA), as well as natural parts like amide practical gatherings from the protein constituents of bone, i.e., collagen [12]. Comparing their results for WH with the FTIR spectrum of powders obtained using doloma in this study, it can be observed that only peaks corresponding to WH are present.

SEM images of sintered pellet samples had lower surface roughness (Figure 5). Figure 6 shows the SEM micrograph and energy-dispersive X-ray spectroscopy (EDS) patterns that confirmed the formation of the whitlockite phase. Since substitutions with smaller ions cause lattice strain, it favors contraction while also stabilizing the structure. This was demonstrated by SEM images (Fig 5): due to the higher volumetric contraction of sintered samples, a different level of densification was observed, resulting in a variation in surface microporosity between 900°C and 1200°C sintered samples [13]. Open pores of the samples present on the sample surface contributed to better bioactivity of the samples.

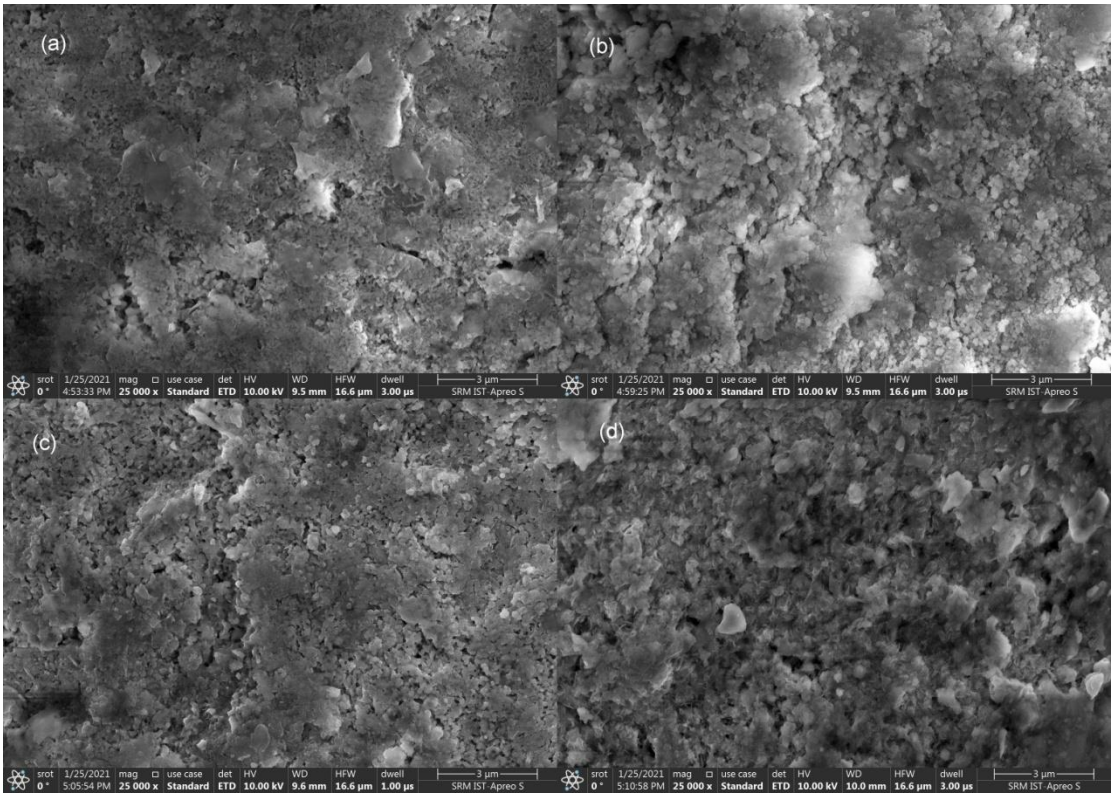

Figure 5.SEM images of samples sintered at temperature from (a) 900°C, (b)1000°C, (c)1100°C and (d) 1200°C

https://doi.org/10.37896/pd91.3/9134

ISSN: 0369-8963

The green densities of the samples were measured from dimensions and sintered samples were measured by Archimedes's principles. Figure 7a showed increase in density with increase in sintering temperature. The densification can be attributed to the grain coarsening during the sintering process at higher temperatures. The decrease in open porosity of the samples can be observed in the SEM images (Fig.5). The density of sintered sample at 900°C was lower and was 1.66g/cc. At the sintering temperature of 1200°C, density of the sample was 1.90g/cc which was the highest. A nearly proportional increase in hardness of the sample (Fig. 7a) can also be observed, with increase in sintering temperature.

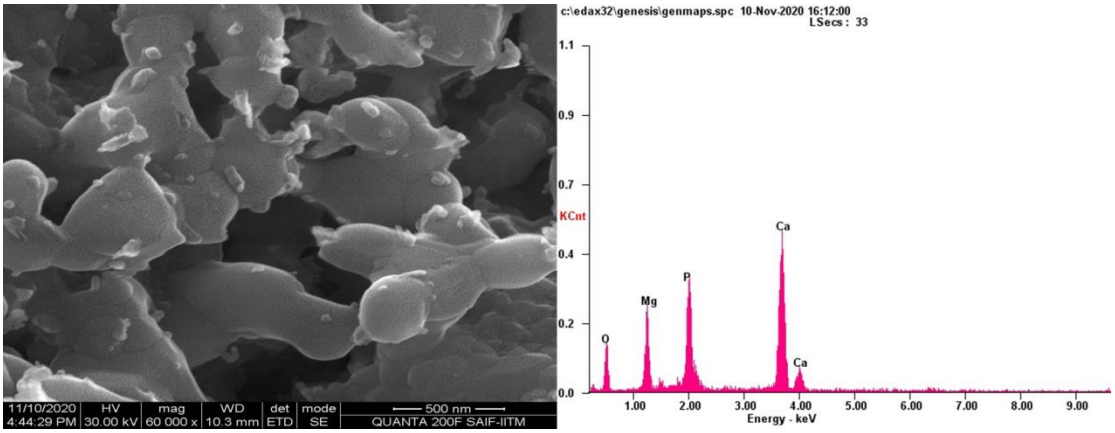

Figure 6.SEM-EDAX images of samples sintered at temperature 1200°C

Antibacterial activity of the sintered samples is shown in Figure.7(b) .The zone of inhibition was calculated for the prepared samples. The zone of inhibition of 900°C sintered sample was 17.8mm and it decreased with increase in the sintering temperature. The maximum zone of inhibition of 1200°C sintered sample was 17.4 mm. The Mg^{2+} ions in the precipitated samples are responsible for the effective antibacterial activity against the E. Coli [17].

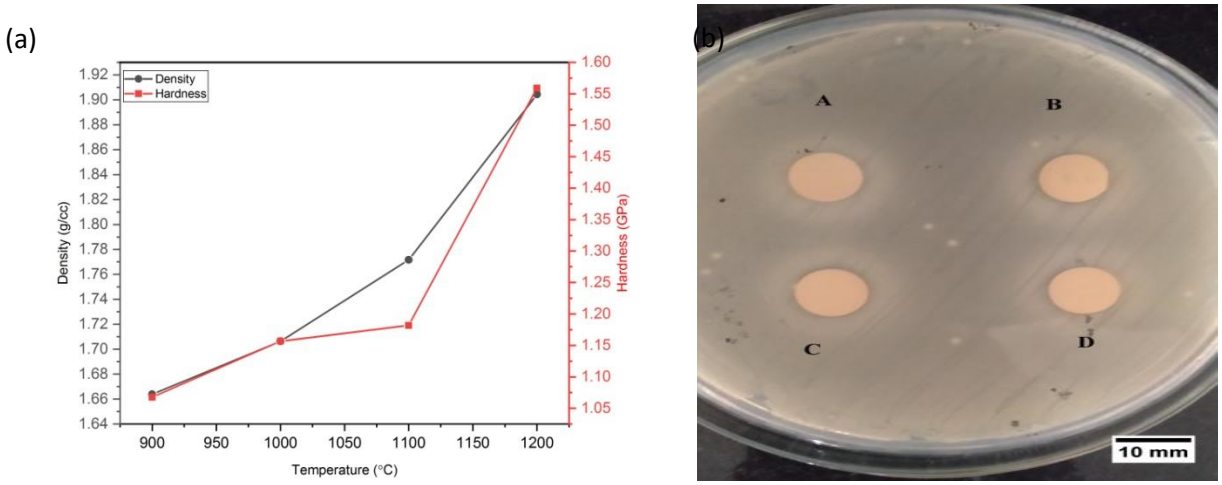

Figure 7. (a) Density and hardness of the heat treated samples, (b) Anti-bacterial test done with E.Coli bacteria

https://doi.org/10.37896/pd91.3/9134

ISSN: 0369-8963

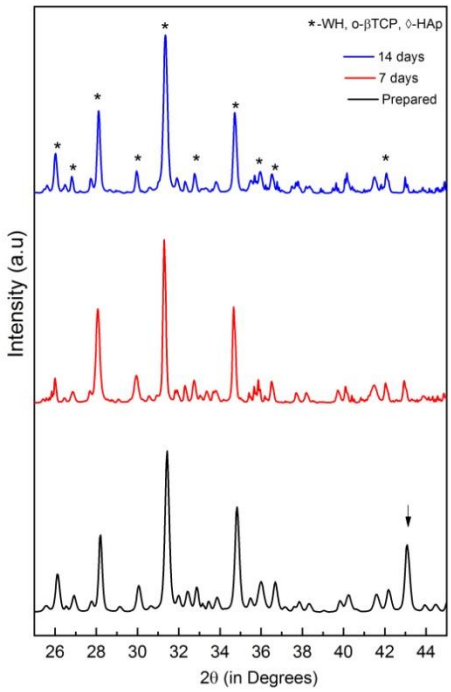

Figure 8. XRD of samples soaked in HBSS solution for 7 and 14 days

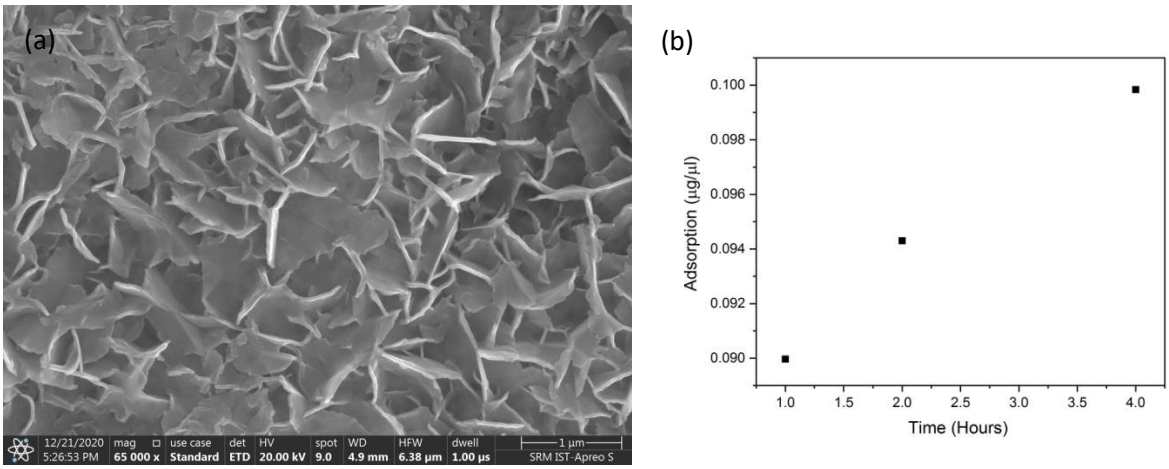

Figure 9. (a) SEM images of soaked in HBSS solution for 14days, (b) Protein adsorption of 1200°C samples

Figure 8 shows the XRD pattern of 1200°C sintered samples after immersion in HBSS solution for 7 and 14 days, and comparison with the unsoaked samples sintered at 1200°C. The peak at 31.2° in sintered samples shifted to low angles in samples soaked in HBSS solutions. The peak at 43.2° disappeared in samples soaked for 14 days. The SEM images of 1200°C sintered sample immersed in HBSS for 14 days is shown in Figure.9a. The apatite layer formation on the surface of the samples can be observed in the SEM images. The calcium ions concentrations increased while samples were immersed in the SBF solution. Meanwhile the Mg^{2+} ions concentration was decreased on the surface of the samples which confirms the dissolution of Mg^{2+}

 https://doi.org/10.37896/pd91.3/9134

ISSN: 0369-8963

ions and deposition of the apatite on the surface of the samples. This result may be related to the precipitation or secondary nucleation of apatite crystals. These findings indicate excellent bioactivity of samples, and, that it promoted the formation of more homogenous layer [14,15]. Figure 9b demonstrates the aggregate sum of protein adsorbed on 1200°C sintered samples. The adsorption of BSA on WH was carried out for 1, 2 and 4 hours. Grain boundaries and presence of rough and microporous surface are potentially favourable for protein adsorption [16]. As can be seen in Fig 9b, the 1200°C sintered samples showed increase in protein adsorption with increasing time.

Conclusions

$Ca_{18}Mg_2H_2(PO_4)_{14}$ was synthesized by precipitation method using doloma without adding external magnesium source and via conventional heat treatment. WH was successfully prepared with high temperature stability and lower amount of HA. FTIR spectrum confirmed presence of CaP group. All the samples predominately had phosphate peaks in FTIR spectra which supported the phosphate based phases obtained by XRD analysis. The microstructure of the samples were analysed by SEM and the samples were found to have spherical particles and open pores were present in the sample surface. The density and hardness of the samples sintered at 1200°C values were 1.9g/cc and 1.55GPa respectively. Apatite formation on the surface of the sample on its immersion in HBSS was confirmed by the SEM images. Antibacterial activity of the samples was observed to be effective against the *E. Coli*. The protein adsorption analysis showed the adhesion property of the surface. Predominate presence of WH at 1200°C sintered samples prepared in this synthesis method proves that the above method can be effectively used to synthesis WH commercially at low cost.

References

1. H.L. JANG, K. JIN, J. LEE, Y. KIM, S.H. NAHM, K.S. HONG, K.T. NAM, *ACS Nano* **8** 634–641 (2014).
2. J. VORMANN, M. ANKE, *J. Clin. Basic Cardiol*. 5 49–53 (2002).
3. S. CASTIGLIONI, A. CAZZANIGA, W. ALBISETTI, J.A. MAIER, *Nutrients* **5** 3022–3033 (2013).
4. CALIFENG WAGN, KI-JAE JEONG, HEE JEONG PARK, MIRIM LEE, SU-CHAK RYN, DAE YOUN HWANG, KYOUNG HYUP NAM, IN HO HAN, JAEBEOM LEE, *Journal of Colloid and Interface Science* 569 1–11 (2020).
5. S. GALLI, Osteoporos.*Int.* **29** 1005–1006 (2018).
6. F.BOUZERARA, A.HARABI, S.ACHOURAA.LARBOT, *Journal of the European Ceramic Society*, **26** [9] 1663-1671 (2006) .
7. HASSAN GHEISARI DEHSHEIKH, SALMAN GHASEMI-KAHRIZSANGI EBRAHIM KARAMIAN, FAZLOLLAH SHAHMOHAMMADIAN, *Ceramics International*, **45**[6] 7390-7396 (2019).
8. ILGEN, O, *Fuel Processing Technology* **92**, 3, 452–455 (2011)
9. HYUN-SEUNG RYU, KUG-SUN HONG, JUNG-KUN LEE, DEUG JOONG KIM, JAE HYUP LEE, BONG-SOON CHANG, DONG-HO LEE, CHOON-KI LEE & SUNG-SOO CHUNG 2004, *Biomaterials*, Volume 25, Issue 3, pp.393-401.

 https://doi.org/10.37896/pd91.3/9134

ISSN: 0369-8963

10. SADAF BATOOL, ZAKIR HUSSAIN, USMAN LIAQAT, MANZAR SOHAIL, Ceramics International **48**,10, 13850-13854 (2022).
11. KRISTINE SALMA, LIGA BERZINA-CIMDINA, NATALIJA BORODAJENKO, *Processing and Application of Ceramics* **4** [1] 45–51 (2010).
12. M. YOUNESI, S. JAVADPOUR, AND M.E. BAHROLOLOOM, *JMEPEG* **20**:1484–1490 (2011).
13. DÉBORA DOS SANTOS TAVARES, LETICIA DE OLIVEIRA CASTRO, GLORIA DULCE DE ALMEIDA SOARES, GUTEMBERG GOMES ALVES, JOSÉ MAURO GRANJEIRO, *Journal of applied oral science,* **21**(1):37-42, (2013).
14. ARNOLD W.G. NIJHUIS, SHINJI TAKEMOTO, M. REZA NEJADNIK, YUBAO LI, XIA YANG, DMITRI A. OSSIPOV, JONS HILBORN, ANTONIOS G. MIKOS, MASAO YOSHINARI, JOHN A. JANSEN &SANDER C.G. LEEUWENBURGH, *Tissue engineering: Part C*, **20**, 10, 838-50 (2014).
15. MENDES, L. S, SASKA1, S, COELHO, F, T. S. DE O. CAPOTE, SCAREL-CAMINAGA, MARCHETTO, R. M, R, CARRODEGUAS, R.G, GASPAR, A. M. M & RODRÍGUEZ, M. A, *Biomedical Materials*, **13**, 2 (2017).
16. JEROME SOHIER, GUY DACULSI, SOPHIE SOURICE, KLAAS DE GROOT AND PIERRE LAYROLLE 2009, *Journal of Biomedical Materials Research Part A*, pp.1105 - 1114.
17. ALEXANDRE M. EMELYANENKO, ALEXANDER G. DOMANTOVSKY, VALERY V. KAMINSKY, IVAN S. PYTSKII., KIRILL A. EMELYANENKO . AND LUDMILA B. BOINOVICH, *Materials* **14**, 5454, (2021)

 https://doi.org/10.37896/pd91.3/9134